Renewable Energy 195 (2022) 1001–1014

Contents lists available at ScienceDirect

Renewable Energy

journal homepage: www.elsevier.com/locate/renene

Dynamic models for air-breathing and conventional polymer electrolyte fuel cells: A comparative study

Fatma Calili-Cankir [a, b], Mohammed S. Ismail [a, c, *], Mohamed R. Berber [d, **], Ziyad A. Alrowaili [e], Derek B. Ingham [a], Kevin J. Hughes [a], Lin Ma [a], Mohamed Pourkashanian [a, c]

[a] Energy 2050, Department of Mechanical Engineering, Faculty of Engineering, University of Sheffield, Sheffield, S3 7RD, United Kingdom
[b] Department of Energy Systems Engineering, Iskenderun Technical University, Hatay, 31 200, Turkey
[c] Translational Energy Research Centre, University of Sheffield, Sheffield, S9 1ZA, United Kingdom
[d] Chemistry Department, College of Science, Jouf University, Sakaka, 2014, Saudi Arabia
[e] Physics Department, College of Science, Jouf University, Sakaka, 2014, Saudi Arabia

ARTICLE INFO

Article history:
Received 14 January 2022
Received in revised form
6 June 2022
Accepted 18 June 2022
Available online 22 June 2022

Keywords:
Air-breathing PEFCs
Conventional PEFCs
Dynamic model
Transient response
Load alterations

ABSTRACT

Two dynamic models have been built for air-breathing and conventional polymer electrolyte fuel cells (PEFCs) in order to comparatively investigate the impacts of some key parameters on the transient response to load alterations and the steady-state performance for each fuel cell type. It was found that with load alterations, the dynamic response of the air-breathing PEFC is significantly slower than that of the conventional PEFC and this is due to significantly slower heat transfer coefficients associated with natural convection taking place at the surface of the exposed-to-the ambient cathode GDL. Namely, lower heat transfer coefficient results in poor heat dissipation that eventually leads to: significantly higher and less-responsive-to-load changes cell temperature (compared to those of the conventional PEFC) and subsequently higher ohmic and activation losses. Further, the dynamic and the steady-state performance of the air-breathing PEFC was found to increase with decreasing GDL porosity, decreasing membrane thickness and, to a lesser extent, decreasing overall electrical resistance. These effects are significantly less profound on the performance of the conventional PEFC. All the above findings have been described and discussed in the paper.

1. Introduction

Polymer electrolyte fuel cells (PEFCs) are promising clean power conversion technologies for a multitude of portable, automotive and stationary applications as they feature high efficiency and rapid start-up [1–5]. Conventional PEFCs typically require some auxiliary components (e.g. fans, compressors and humidifiers) to supply and humidify the reactant gases. These auxiliary components bring additional weight and volume and increase the cost of entire fuel cell system. Focusing on power sources for small portable devices, the number of the auxiliary components should be minimised to allow for significant size reduction of the fuel cell system and subsequently compete with the conventionally used non-environmentally friendly batteries [6–8]. In air-breathing PEFCs, the cathode is open to the ambient, and this means that the cathode gas diffusion layer is in direct contact with the ambient, and that oxygen (required for the oxygen reduction half reaction at the cathode electrode) and water vapour (required for the initial humidification of the membrane electrolyte) are directly extracted from the ambient air through natural convection [9–11]. To this end, storage, pumping and humidifying devices are no longer required for the cathode sides of the fuel cell, thus significantly simplifying the fuel cell system. However, the performance of the air-breathing PEFC is significantly inferior to that of the conventional PEFC. Evidently, this is due to the substantially lower heat and mass transfer coefficients associated with natural convection at

* Corresponding author. Energy 2050, Department of Mechanical Engineering, Faculty of Engineering, University of Sheffield, Sheffield, S3 7RD, United Kingdom.
** Corresponding author.
E-mail addresses: m.s.ismail@sheffield.ac.uk (M.S. Ismail), mrberber@science.tanta.edu.eg (M.R. Berber).

https://doi.org/10.1016/j.renene.2022.06.092

Nomenclature

Roman symbols

a	Water activity [−]
A_{act}	Active area of the fuel cell [m^2]
$D^{eff}_{H_2O}$	Effective diffusivity of water into air [m^2/ s]
$D_{H_2O,air}$	Binary diffusivity of water into air [m^2/s]
$D^{eff}_{O_2}$	Effective diffusivity of oxygen into air [m^2/ s]
$D_{O_2,air}$	Binary diffusivity of oxygen into air [m^2/ s]
E	Nernst Voltage [V]
E_0	Standard fuel cell voltage [V]
F	Faraday's constant [C/mol]
j	Current density [A/m^2]
j_0	Exchange current density [A/m^2]
I	Electric current [A]
k_{an}	Anode valve constant [$\sqrt{mol.g}$/(atm.s)]
k_{ca}	Cathode valve constant [$\sqrt{mol.g}$/(atm.s)]
K_{H_2}	Hydrogen valve constant [mol/(atm.s)]
K_{H_2O}	Water valve constant [mol/(atm.s)]
K_{O_2}	Oxygen valve constant [mol/(atm.s)]
M	Molar mass [g/mol]
n	Number of moles
P	Ambient pressure [atm]
P_{H2}	Partial pressure of hydrogen [atm]
P_{H_2O}	Partial pressure of water vapour [atm]
P_{sat}	Water vapour saturation pressure [atm]
P_{O_2}	Partial pressure of oxygen [atm]
q_{H_2}	Hydrogen molar flow [mol/s]
R	Universal Gas Constant [atm/(mol.K)]
RH	Relative humidity [%]
R_{elec}	Lumped electrical cell resistance [Ω]
R_{mem}	Membrane resistance [Ω]
T	Absolute temperature [K]
U	Utilization factor [−]
V_{an}	Anode volume [m^3]
V_{ca}	Cathode volume [m^3]
V_{cell}	Cell voltage [V]
x	Mole fraction [−]

Greek symbols

α	Charge transfer coefficient [−]
δ	Thickness [m]
ε	Porosity [−]
η_{act}	Activation over voltage [V]
η_{ohmic}	Ohmic over voltage [V]
λ	Water content [−]
σ_{mem}	Ionic conductivity [S/m]
τ	Tortuosity [−]
τ_{H_2}	Hydrogen time constant [s]
τ_{H_2O}	Water time constant [s]
τ_{O_2}	Oxygen time constant [s]

the open cathode of the air-breathing PEFC (compared to those of the cathode flow channels of the conventional PEFC or an open cathode with an integrated fan). This often leads to inadequate heat and mass exchange between the cathode catalyst layer and the ambient [12].

In the past two decades, there has been research work that has compared the effects of the natural and forced convection on the performance of the PEFCs. Santa Rosa et al. [13] developed an eight-cell air-breathing PEFC stack in order to investigate the difference between forced air-convection and natural air convection. They reported that the fuel cell performance with forced air convection is, for a typical voltage (i.e. 4 V), more than two times higher than the one with natural convection. Fernandez-Moreno et al. [14] built a portable system using an air-breathing PEFC for power generation and tested it with and without using a cathodic fan. They showed that the use of fan mitigated water flooding at the cathode of the fuel cell and the maximum current density of the PEFC with the fan is 0.37 A/cm^2 while it is 0.24 A/cm^2 if the operation of the fuel only relies on natural convection. Ferreira-Aparicio and Chaparro [15] studied different cathode designs to optimise the cathode architecture to reduce mass transport resistance of an air-breathing PEFC. Enlighten by performance tests that were performed under natural and forced convection conditions, they showed the importance of the cathode design on the performance of the air-breathing PEFCs. Namely, as the opening of the open cathode collector increases, the cell performance in general improves. Jung et al. [16] added hydrophilic silica nano-particles to the anode catalyst layer to improve water management in air-breathing and air-blowing PEFCs. They showed that the proposed method improved the performance of both air-breathing and air-blowing PEFCs by around 27% and 44%, respectively. Ous and Arcoumanis [17] examined the effect of air stoichiometry on the formation of the water droplets under natural and forced convections in an PEFC with open cathodes. They observed that there was no droplet formation for the first 5 min at the lowest reported current density (i.e. 80 mA/cm^2) and then small and few droplets formed under natural convection. However, the current density almost doubled and that the number and size of droplets significantly increased when a fan was operated to provide increased air flow rates. Calili-Cankir et al. [18] developed two mathematical steady-state models for air-breathing and conventional PEFCs to conduct a parametric investigation on how natural convection affects the performance of the air-breathing PEFC. They showed that the conventional PEFC outperforms the air-breathing PEFC and this is due to the substantially higher heat and mass transfer coefficients associated with the former fuel cell type. They also found that the air-breathing PEFC is, compared to the conventional PEFC, more sensitive to the membrane thickness and less sensitive to the electrical conductivity.

However, there have been no studies that have thoroughly investigated the effect of natural convection on the transient response of the air-breathing PEFC. Air-breathing PEFCs should be reasonably responsive to the rapid and/or high load variations in order to meet the power requirements of the small electronic devices. In a previous work [19], we investigated the transient response of the air-breathing PEFC at different ambient conditions (temperature and relative humidity), GDL parameters (thickness and thermal conductivity) and hydrogen utilization. In this study, two dynamic models for air-breathing and conventional PEFCs have been developed within the platform of MATLAB/Simulink to investigate, for the first time, the effect of natural convection on the transient response of the air-breathing PEFC by simultaneously comparing with the outcomes of both dynamic models. Furthermore, the effects of the GDL porosity, the membrane thickness and the electrical resistance on the transient response of both types of fuel cells have been comparatively assessed in this study to provide better insights on how some key design parameters should be varied to improve the dynamic response of the air-breathing PEFC.

2. Dynamic modelling of fuel cells

2.1. Model assumptions

Two dynamic models for single air-breathing and conventional PEFCs are developed within the platform of MATLAB/Simulink. The modelled air-breathing PEFC was originally described and reported by Fabian and his co-workers [20] and the geometry and the physical parameters of the conventional PEFC have been considered to be the same as those of the air breathing PEFC; see Table 1. Fig. 1 demonstrates the schematic representations of key components of the fuel cells modelled in this study. It should be noted that we have not listed the dimensions of the hydrogen chamber (for the air-breathing PEFC) and the flow channels (for the conventional PEFC) in Table 1 as they were not used in the calculations; the concentrations and temperature at the surfaces of the GDLs were assumed to be the same as those of the chamber and the flow channels. The following assumptions and considerations have been taken into account for the developed dynamic models:

- Water exists only in vapour form.
- The reactant gases are ideal.
- The anode is dead-ended in the air-breathing PEFC.
- The catalyst layers are treated as interfaces between the membrane and the GDLs as they are infinitely thin.
- The water activity within the membrane is in equilibrium with water vapour activity in the catalyst layers.
- The properties of all the fuel cell components are assumed to be uniform.

As shown in Fig. 2, the dynamic models, expressed in the Laplace domain, consist of three main blocks: Nernst voltage, activation losses and ohmic losses. The outputs of the models are the cell voltage and power. It has been previously reported that the sharp decline in the cell voltage of the modelled air-breathing PEFC at high current densities was found to be primarily due to the membrane dehydration [19–22]; hence, we assume that, for simplification and comparative purposes, the concentration losses, typically induced by water flooding and/or insufficient supply of the reactant gasses to the catalyst layers at high current densities, are negligible for the dynamic models. The 'Cell Temperature' block in Fig. 2 is a link to steady-state models for the fuel cells that were built in a previous work [18] in order to feed the dynamic models with the temperature of the cathode catalyst layer. The steady-state models were called as a function in the dynamic models that runs these steady-state models for a given set of parameters and operating conditions and curve-fits the temperature-current density data in order to use the corresponding curve-fitting equation as an input for the dynamic models. This temperature was treated as the cell temperature; this is a reasonable approximation as: (i) the temperature of the cathode catalyst layer is the highest compared to other parts of the fuel cell and (ii) the temperature variation across the fuel cell is normally less than 2 °C [18]. It is noteworthy that the details of the steady-state models were not mentioned in the present study in order to maintain flow of the paper and to avoid distracting readers from its main focus, which is the transient response of the fuel cells; the interested readers are referred to Ref. [18] for further details regarding the steady-state models.

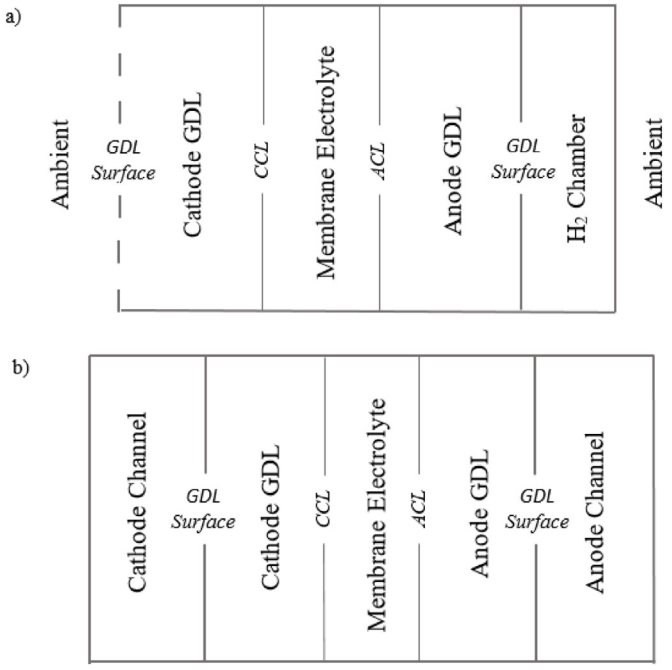

Fig. 1. Schematic diagrams of the modelled: (a) air-breathing and (b) conventional PEFCs (adapted from Ref. [18]). Note that the abbreviations 'CCL' and 'ACL' stand for cathode catalyst and anode catalyst layers respectively. The dimensions of the key components are listed in Table 1.

Table 1
Physical parameters and constants used in the dynamic models [19].

Parameters	Value
Universal gas constant, R	8.315 J/(mol.K)
Faraday's constant, F	96500 C/mol
Standard reversible fuel cell voltage, E_0	1.23 V
Ambient/cell pressure, P	1 atm
Ambient temperature, T_∞	20 °C
Initial cell temperature of conventional PEFC, T	20 °C
Binary diffusivity of O_2 in air, $D_{O_2\,air}$	2.1×10^{-5} m^2/s
Binary diffusivity of H_2O in air, $D_{H_2O,air}$	2.6×10^{-5} m^2/s
Length of active cell side (square), L_a	0.03 m
Cell active area, A_{act}	0.0009 m^2
Membrane thickness, δ_{mem}	5.2×10^{-5} m
GDL thickness, δ_{gdl}	3.0×10^{-4} m
GDL porosity, ε	0.4
GDL tortuosity, τ	3.0
GDL thermal conductivity, k_{gdl}	10 W/(m.K)
Exchange current density, j_0	2.5×10^{-5} A/cm^2
Lumped cell electrical resistance, R_{elec}	12 mΩ
Charge transfer coefficient, α	0.28
Utilization factor, U	0.7
Hydrogen time constant, τ_{H_2}	0.3096 s
Oxygen time constant, τ_{O_2}	0.7784 s
Water vapour time constant, τ_{H_2O}	0.9288 s
Hydrogen valve constant, K_{H_2}	3.627×10^{-5} mol/(s.atm)
Oxygen valve constant, K_{O_2}	1.443×10^{-5} mol/(s.atm)
Water vapour valve constant, K_{H_2O}	1.209×10^{-5} mol/(s.atm)

2.2. Model formulation

The cell potential for both types of fuel cells, V_{cell}, is calculated as follows [23]:

$$V_{cell} = E - \eta_{act} - \eta_{ohmic} \quad (1)$$

where E is the Nernst (the reversible) voltage and η_{act} and η_{ohmic} are the activation and ohmic losses, respectively. As shown below, the equations used for each dynamic model were compiled in a subsection to avoid confusion starting with those specific to air-breathing PEFCs. Where equations are common for both fuel cell types, the necessary notes and references are given in the conventional PEFC subsections.

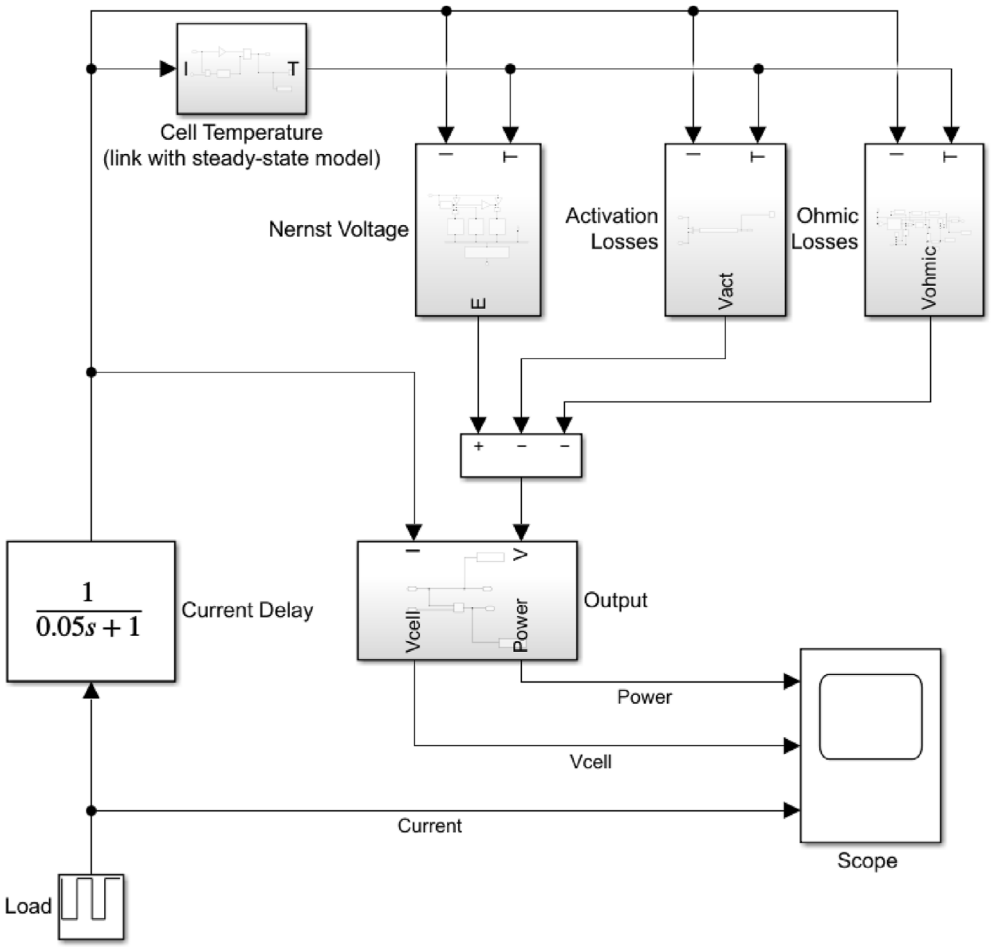

Fig. 2. The block diagram of the dynamic model for the fuel cells.

2.2.1. Air-breathing PEFC

The Nernst voltage is obtained by Ref. [24]:

$$E = E_0 + \frac{RT}{2F}\ln\left(P_{H_2}.P_{O_2}^{1/2}\right) \tag{2}$$

where E_0 is the standard reversible fuel cell voltage, T is the absolute temperature, R is the universal gas constant and F is the Faraday's constant. P_{H_2} and P_{O_2} are the partial pressures of hydrogen and oxygen, respectively. Fig. 3 illustrates the block diagram of the Nernst voltage for the air-breathing PEFC.

The partial pressure of oxygen in the open cathode compartment is calculated by Refs. [19,25]:

$$P_{O_2} = x_{O_2}P = x_{O_2}^0 - \delta_{GDL}\frac{jRT}{4FD_{O_2}^{eff}} \tag{3}$$

where $x_{O_2}^0$ is the mole fraction of the oxygen in the ambient air (i.e. 0.21), δ_{GDL} is the GDL thickness, j is the current density and P is the ambient pressure. The effective diffusivity of oxygen into air $D_{O_2}^{eff}$, is calculated using the following expression:

$$D_{O_2}^{eff} = \frac{\varepsilon}{\tau}D_{O_2,air} \tag{4}$$

where ε and τ are the porosity and tortuosity of the porous diffusion medium, respectively and $D_{O_2,air}$ is the binary diffusivity of oxygen into air.

The relationship of the hydrogen molar flow through a valve with its partial pressure inside the flow channel can be expressed as follows [26]:

$$\frac{q_{H_2}}{P_{H2}} = \frac{k_{an}}{\sqrt{M_{H_2}}} = K_{H_2} \tag{5}$$

where k_{an} and K_{H_2} are the anode valve constant and the molar valve constant for hydrogen, respectively. M_{H_2} is the molar mass of hydrogen. The derivative of the partial pressure of hydrogen is determined using the ideal gas law and written in the Laplace transform domain as follows [26]:

$$P_{H_2}V_{an} = n_{H_2}RT \tag{6}$$

where V_{an} and n_{H_2} are the volume of the anode compartment and the number of hydrogen moles in the anode channel, respectively. The time derivation of Eq. (6) can be obtained by:

$$\frac{d}{dt}P_{H_2} = \frac{RT}{V_{an}}q_{H_2} \tag{7}$$

where q_{H_2} is the molar flow rate of hydrogen and given by:

$$q_{H_2} = q_{H_2}^{in} - K_{H_2}P_{H_2} - q_{H_2}^{r} \tag{8}$$

where $q_{H_2}^{in}$ and $q_{H_2}^{r}$ are the inlet flow rate of hydrogen and the flow rate of reacting hydrogen, respectively.

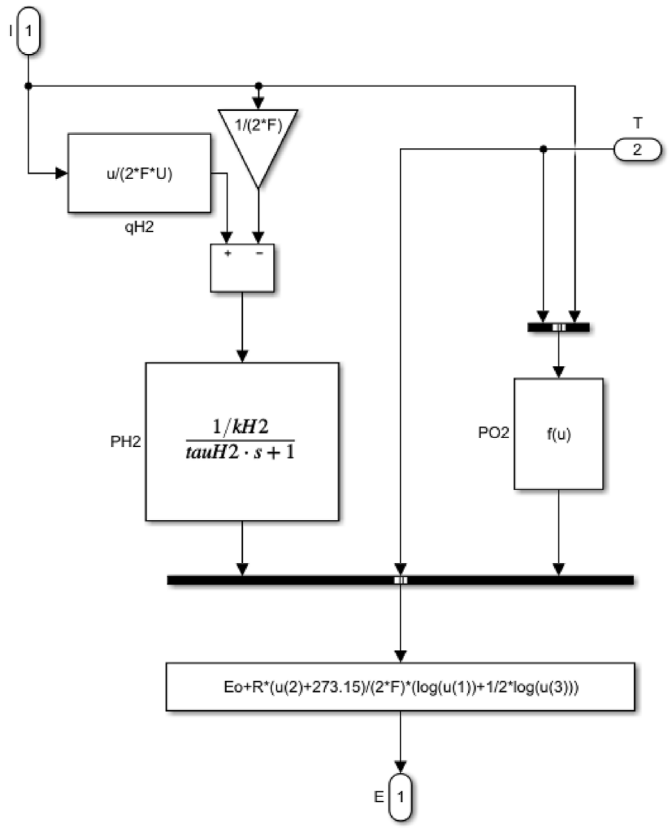

Fig. 3. The block diagram of the Nernst voltage for the air-breathing PEFC.

The molar flow rate of reacting hydrogen can be obtained as a function of the fuel cell current I using Faraday's second law of electrolysis:

$$q_{H_2}^r = \frac{I}{2F} \tag{9}$$

After substituting Eq. (8) and Eq. (9) into Eq. (7), the derivation of partial pressure of oxygen can be rewritten as follows:

$$\frac{d}{dt}P_{H_2} = \frac{RT}{V_{an}}\left(q_{H_2}^{in} - K_{H_2}P_{H_2} - \frac{I}{2F}\right) \tag{10}$$

And its expression in the Laplace domain [19,25]:

$$P_{H_2} = \frac{1/K_{H_2}}{1+\tau_{H_2}s}\left(q_{H_2}^{in} - \frac{I}{2F}\right) \tag{11}$$

The hydrogen time constant τ_{H_2}, is given by:

$$\tau_{H_2} = \frac{V_{an}}{K_{H_2}RT} \tag{12}$$

The activation losses are expressed as follows [19]:

$$\eta_{act} = \frac{RT}{2\alpha F}\ln\left(\frac{j}{j_0}\right) \tag{13}$$

where α and j_0 are the charge transfer coefficient and the exchange current density, respectively. Note that the exchange current density is a function of temperature as evident from Eq. (13) in Ref. [19]. The exchange current density shown in Table 1 was obtained after correcting the reference exchange current density at 30 °C (i.e. 5×10^{-5} A/cm^2) for the temperature which is initially 20 °C in our case. However, for simplification, the sensitivity of the exchange current density to temperatures beyond 20 °C was assumed to be negligible. Relaxing this assumption was found to result in an almost negligible impact on the performance of the modelled fuel cells at the selected currents (an increase up to 0.03 for the air-breathing PEFC and up to 0.01 V for the conventional PEFC).

The ohmic losses can be obtained using the equation [22]:

$$\eta_{ohmic} = jA_{act}(R_{elec} + R_{mem}) \tag{14}$$

where A_{act} is the active area of the fuel cell and R_{elec} is the lumped electrical resistance of the cell. The membrane resistance, R_{mem}, is defined as follows:

$$R_{mem} = \frac{\delta_{mem}}{A_{act}\sigma_{mem}} \tag{15}$$

where δ_{mem} is the thickness of the polymer electrolyte membrane. The ionic conductivity of the membrane, σ_{mem}, can be calculated using following empirical expression that is more appropriate for air-breathing PEFC than the well-known Springer's model [27]:

$$\sigma_{mem} = \left(3.46a^3 + 0.0161a^2 + 1.45a - 0.175\right)\exp\left[1268\left(\frac{1}{303} - \frac{1}{T}\right)\right] \tag{16}$$

where a is the water activity and given by Ref. [24]:

$$a = \frac{P_{H_2O}}{P_{sat}} \tag{17}$$

where P_{H_2O} and P_{sat} are the partial pressure and saturation pressure of water vapour at the cell temperature, respectively. The partial pressure of water is obtained as follows [19,25]:

$$P_{H_2O} = x_{H_2O}P = x_{H_2O}^0 + \delta_{GDL}\frac{jRT}{2FD_{H_2O}^{eff}} \tag{18}$$

where $x_{H_2O}^0$ is the mole fraction of the water vapour in the ambient air as a function of ambient relative humidity (RH) and $D_{H_2O}^{eff}$ is the effective diffusivity of water into air. These quantities are obtained as follows:

$$x_{H_2O}^0 = \frac{RH \times P_{sat}}{100} \tag{19}$$

and

$$D_{H_2O}^{eff} = \frac{\varepsilon}{\tau}D_{H_2O,air} \tag{20}$$

The saturation pressure of water vapour is calculated by Ref. [28]:

$$\begin{aligned} log_{10}P_{sat} = &-2.1794 + 0.02953(T - 273.15) \\ &- 9.1837 \times 10^{-5}(T - 273.15)^2 \\ &+ 1.4454 \times 10^{-7}(T - 273.15)^3 \end{aligned} \tag{21}$$

2.2.2. Conventional PEFC

As with the air-breathing PEFC, the relationship between the hydrogen molar flow through a valve and its partial pressure inside the flow channel is given by Eq. (5). The detailed derivation of the

partial pressure of hydrogen in the Laplace transform domain is shown in Eqs 6–11.

Similarly, it may be considered that the molar flows of oxygen (q_{O_2}) and water vapour (q_{H_2O}) through the valve are proportional to their partial pressures inside the flow channel of the fuel cell. The valve molar constants of oxygen (K_{O_2}) and water (K_{H_2O}) can be obtained as follows:

$$\frac{q_{O_2}}{P_{O2}} = \frac{k_{ca}}{\sqrt{M_{O_2}}} = K_{O_2} \tag{22}$$

and

$$\frac{q_{H_2O}}{P_{H_2O}} = \frac{k_{an}}{\sqrt{M_{H_2O}}} = K_{H_2O} \tag{23}$$

where k_{ca} and k_{an} are respectively valve constants of the cathode and anode compartments. M_{O_2} and M_{H_2O} are molar masses of oxygen and water vapour, respectively. P_{O2} and P_{H_2O} are the partial pressures of oxygen and water, respectively.

For oxygen and water, the derivatives of their partial pressures can be obtained using the ideal gas law and rewritten in the Laplace transform domain as follows [29]:

$$P_{O_2} = \frac{{}^1/_{K_{O_2}}}{1 + \tau_{O_2} s}\left(q_{O_2}^{in} - \frac{I}{4F}\right) \tag{24}$$

and

$$P_{H_2O} = \frac{{}^1/_{K_{H_2O}}}{1 + \tau_{H_2O} s}\left(\frac{I}{2F}\right) \tag{25}$$

where τ_{O_2} and τ_{H_2O} are respectively oxygen and water time constants and they can be expressed as follows:

$$\tau_{O_2} = \frac{V_{ca}}{K_{O_2} RT} \tag{26}$$

and

$$\tau_{H_2O} = \frac{V_{an}}{K_{H_2O} RT} \tag{27}$$

The Nernst Voltage for a conventional PEFC can be written as [23]:

$$E = E_0 + \frac{RT}{2F}\ln\left(\frac{P_{H_2}.P_{O_2}^{1/2}}{P_{H_2O}}\right) \tag{28}$$

Using Eqs. (11), (24), (25) and (28), the Nernst voltage of the conventional fuel cell can be depicted as shown in Fig. 4.

The activation and ohmic losses are calculated using Eq. (13) and Eq. (14), respectively. The ionic conductivity of the membrane, σ_{mem}, is estimated using the well-known Springer's model [28]:

$$\sigma_{mem} = [0.514\lambda - 0.326]\exp\left[1268\left(\frac{1}{303} - \frac{1}{T}\right)\right] \tag{29}$$

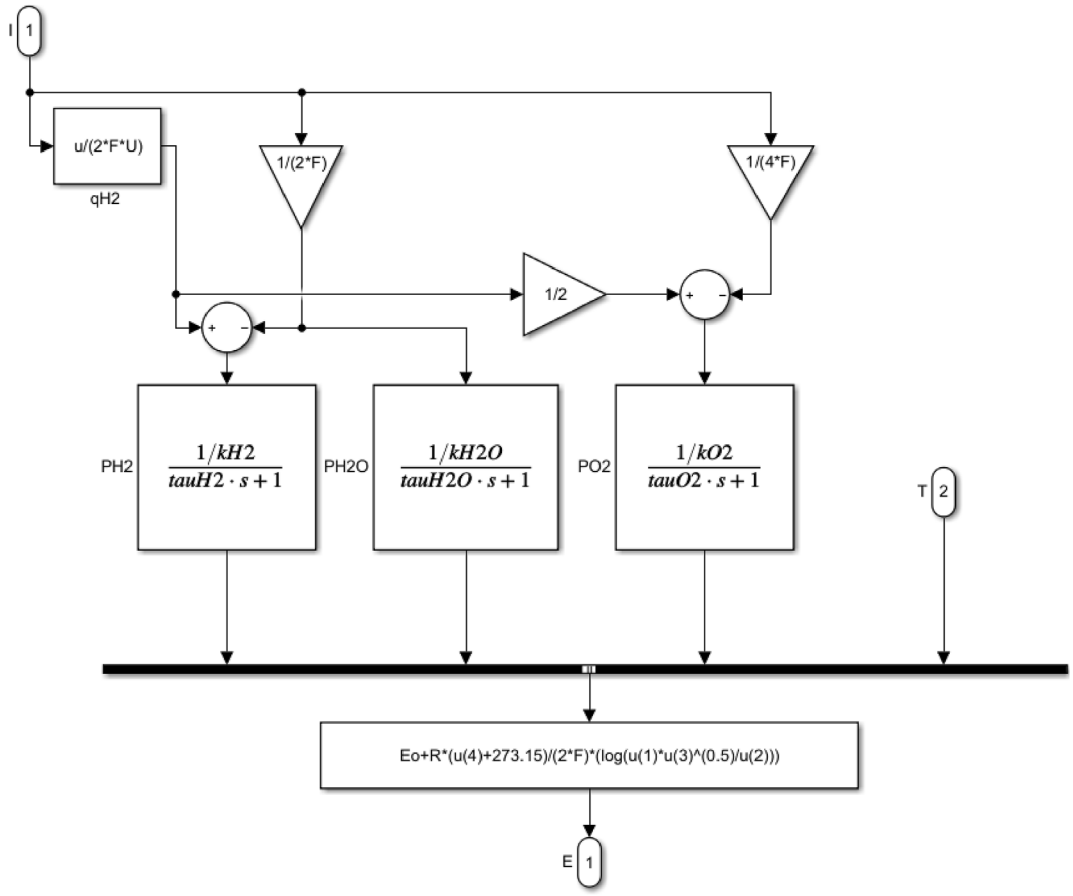

Fig. 4. The block diagram of the Nernst voltage for the conventional PEFC.

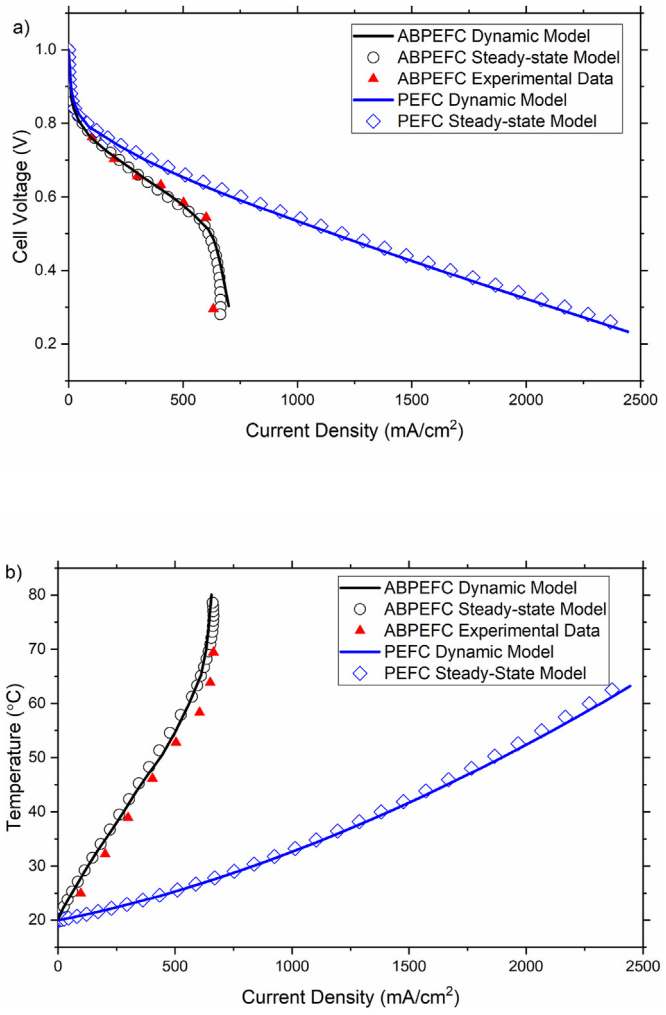

Fig. 5. Dynamic model outputs of the fuel cells against the steady-state modelling data [18] and the experimental data [20] at 20 °C and 40% relative humidity: a) cell voltage and b) cell temperature.

where λ represents the water content of the membrane and is calculated using the following expression:

$$\lambda = \begin{cases} 0.043 + 17.81a - 39.85a^2 + 36a^3, & 0 < a \leq 1 \\ 14 + 1.4(a-1), & 1 < a \leq 3 \end{cases} \quad (30)$$

where a is the water activity which is given in Eq. (17). P_{H_2O} that is required to calculate water activity is estimated using Eq. (25).

3. Results and discussion

Fig. 5 demonstrates the polarisation curves and the surface temperature of the cathode GDL generated by the dynamic models of the fuel cells at 20 °C and 40% relative humidity. The steady-state output of the dynamic model of the air-breathing PEFC is validated against the experimental data reported by Fabian et al. [20]. The sharp decline in the performance and the sharp increase in the GDL surface temperature at high current densities are captured by the dynamic model of the air-breathing PEFC. Fig. 5 also shows that the dynamic modelling data of both type of fuel cells under steady-state conditions are in very good agreement with the corresponding steady-state modelling data previously reported in Ref. [18]. Note that the solution was found to be insensitive to time steps below 0.05 s and as such the latter time step was selected for the simulations.

In the following subsections, we conduct a study to first investigate the impact of type of convection at the cathode side (natural convection for the air-breathing PEFC versus forced convection for the conventional PEFC) on the fuel cell performance. This is followed by a parametric study that investigates the effects of the GDL porosity, the membrane ionic resistance and the electrical resistance on the transient response for each type of the fuel cells. This parametric study is primarily performed in order to: (i) evaluate the impact of natural convection on the transient response of the air-breathing PEFC to sudden and large load changes and (ii) have better insights on how to improve this transient response through refining the investigated parameters (i.e. the GDL porosity, the ionic resistance of the membrane and the overall electronic resistance of the fuel cell).

3.1. Transient operation

Two load current values (i.e. 1 and 5 A) were chosen to simulate a large current step change considering the air-breathing PEFC. The "Repeating Sequence Stairs" built-in function in Simulink was used in order to program rapid load alterations between low and high current steps after each 300 s for 2100 s; 300 s was experimentally found to be sufficient for the potential of the air-breathing PEFC to stabilise [20]. According to Kim et al. [30], the evolution of the cell temperature with time under rapid load alteration is given by:

$$T(t) = T_2 + (T_1 - T_2) \times \exp\left(-\frac{h}{mC_p}t\right) \quad (31)$$

where T_1 and T_2 are the steady cell temperature before and after applying the current step change, respectively. h is the heat transfer coefficient and mC_p is the heat capacitance of the fuel cell.

It should be noted that the cell temperature as a function of current density data were generated for each variable investigated in this study (i.e. convection type, the GDL porosity, the membrane thickness and the overall electrical conductivity) using previously-developed steady-state models reported in Refs. [18,22]. These data were fitted to high order polynomials and directly linked to the corresponding dynamic models so that the steady-state temperatures T_1 and T_2 are supplied and used in Eq. (31); an example of some high-order polynomial curve fitting equations were presented in a previous work [19]. In the earlier work [19], $\frac{h}{mC_p}$ value was estimated as 0.0295 s^{-1} for the air-breathing PEFC. Further, the mean heat transfer coefficients were found to be 41.95 and 103.29 W/(m^2.K) for the air-breathing and conventional PEFCs respectively [18]. To this end, $\frac{h}{mC_p}$ for the conventional PEFC could be estimated as 0.0726 s^{-1}.

Fig. 6 shows that the load current of the fuel cells as it suddenly changes between low (1 A) and high (5 A) currents at 20 °C and 40% relative humidity. The cell temperature for both types of fuel cell follow the sudden load changes and sharply increases/decreases before stabilisation. From the graph, it is clear that the time needed to stabilise cell temperature for the air-breathing PEFC is longer than that of the conventional PEFC.

3.2. Type of convection effect

Fig. 7 shows the impact of convection type (i.e. natural versus forced convection) on the transient response of the fuel cell at typical values of 20 °C and 40% relative humidity. It is clear from the figure that the dynamic response of the conventional PEFC is more stable than the air-breathing PEFC as it (i.e. the air-breathing PEFC) demonstrates substantially less overshoots and faster response

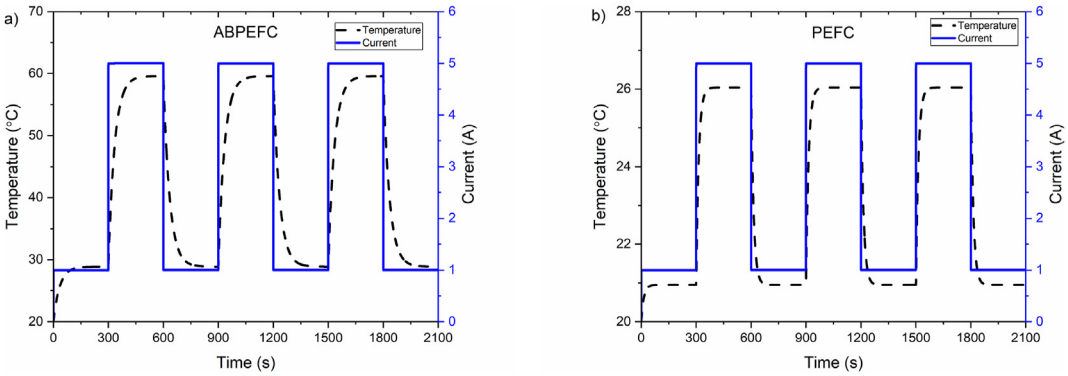

Fig. 6. The cell temperature as it changes with alternating 4-A step changes in the load current under 20 °C and 40% relative humidity for: (a) air-breathing PEFC and (b) conventional PEFC.

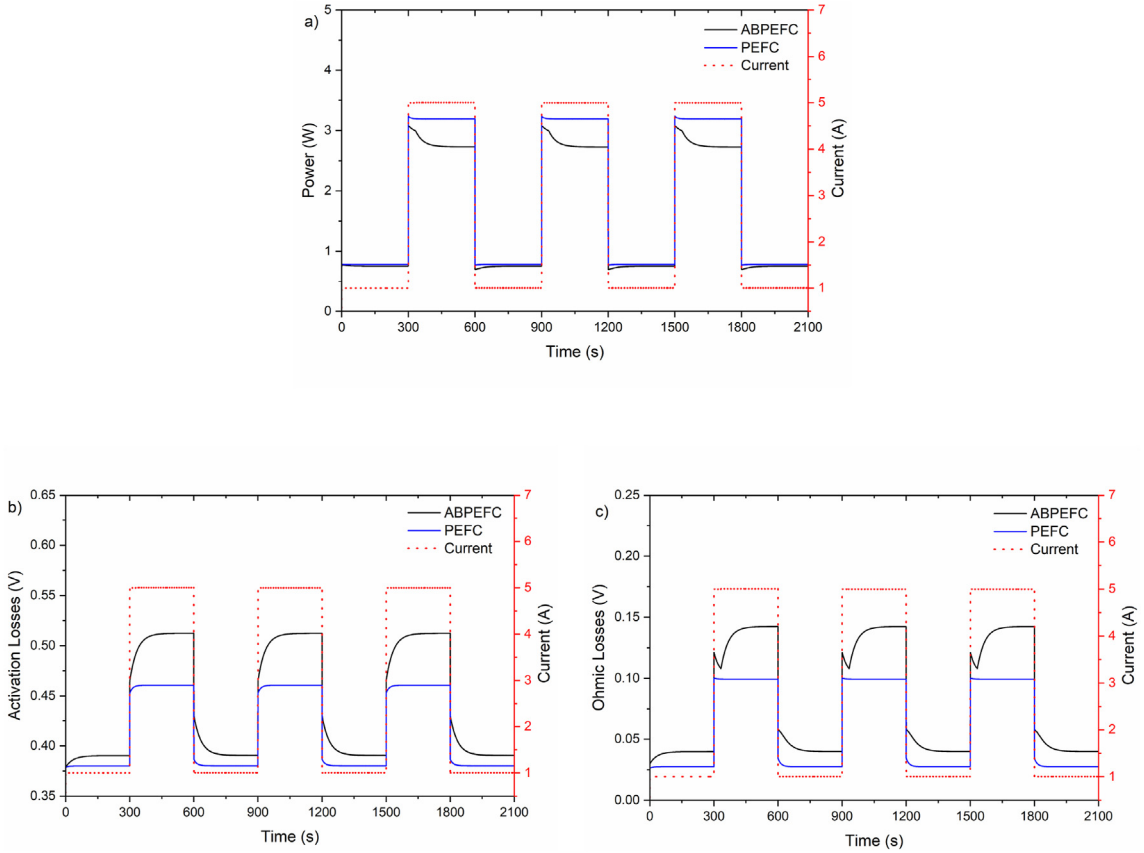

Fig. 7. Transient profiles of the modelled fuel cells for: (a) output power, (b) activation losses and (c) ohmic losses at 20 °C and 40% relative humidity.

times. When the load is step-changed from 1 A to 5 A, the power of air-breathing PEFC sharply increases from 0.75 W to 3.05 W and then stabilises at 2.75 W after around 100 s while the power of the conventional PEFC sharply increases from 0.78 W to 3.25 W and then stabilises at 3.2 W after around 25 s (Fig. 7a). Thus, the time that requires for the air-breathing PEFC to stabilise is about 4 times higher than that of the conventional PEFC when changing from low load (1 A) to high load (5 A). On the other hand, when the load is reversely step-changed from high to low currents, the power of the air-breathing PEFC suddenly decreases from 2.75 W to 0.69 W and then stabilises at 0.75 W while the power of the conventional PEFC sharply decreases from 3.2 W to 0.76 W and stabilises at 0.78 W. The observation that the output power demonstrates significantly higher overshoots than the conventional PEFC is attributed to the profiles of the activation (Fig. 7b) and the ohmic (Fig. 7c) losses. It is seen clearly from these two figures that the activation and the ohmic losses of the air-breathing PEFC are significantly less responsive to load alterations. These dynamic profiles for the activation and ohmic losses (which are both stronger function of temperature as shown in Section 2.2) are linked to the dynamic profiles of the fuel cell temperature (Fig. 6) where the cell temperature of the air-breathing PEFC is significantly higher and less responsive to load changes than the conventional PEFC. This is evidently due to significantly lower heat transfer coefficient at the surface of the open cathode of the air-breathing PEFC compared to that of the cathode flow channel of the conventional PEFC.

It is noteworthy that, when step-changed to 5 A, the ohmic losses associated with the air-breathing PEFC firstly decrease and then increase (Fig. 7c); this is attributed to the two-field effect of the temperature described in our previous work [19]. Namely, when load is suddenly increased to 5 A, the resulting sudden increase in the cell temperature causes an initial increase in the ionic conductivity of the membrane (Eq. (16)) and as such the ohmic losses decreases. As time passes, such a positive impact of the cell temperature on the ionic conductivity is, however, countered by the exponential increase in the saturation pressure of water vapour (Eq. (21)) that eventually decreases the ionic conductivity of the membrane (and increases the ohmic losses) before reaching steady-state values.

3.3. GDL porosity effect

Fig. 8 shows the impact of the GDL porosity on the dynamic and the steady-state performances of the air-breathing PEFC. Note that the porosity of both cathode and anode GDLs have been simultaneously changed with the same values. It should be also noted that, for simplification, the microporous layers (MPLs) were not explicitly considered in the models; they were implicitly accounted for by relatively low GDL porosity values: 0.6 and 0.4. Adding MPLs to the model implies adding a new set of mass and heat transfer equations for the steady-state models; this may provide a marginal gain in terms of prediction accuracy but would unnecessarily complicate the modelling framework. Fig. 8b shows that the overshoots in the output power decrease with decreasing GDL porosity at high currents. In addition, the figure shows the performance of the air-breathing PEFC improves with decreasing porosity; this is more evident with 5 A that with 1 A as the values of and the variation in the ohmic losses are higher in the former case (Fig. 8d). This improvement in the cell performance with decreasing GDL porosity is attributed to the decreased transfer rate of water from the catalyst layer (particularly from the cathode catalyst layer where water is produced) to the surface of the GDL (and then to the ambient) with decreasing GDL porosity. This allows for more water to be available for the humidification of the membrane phase; this is evident from Fig. 8c which shows that the water activity at the cathode catalyst layer increases and demonstrates less overshooting with decreasing porosity. As the water activity of the membrane phase increases, the ionic conductivity increases and the ohmic losses of the cell decreases (Fig. 8d). It should be noted that poor heat dissipation at the cathode of the air-breathing PEFC due to low heat transfer coefficients results in relatively high temperatures (Fig. 8a) which substantially increase the saturation pressures of water vapour and render the water required for membrane humidification a performance limiting factor.

Fig. 9 shows the impact of the GDL porosity on the dynamic and the steady-state performances of the conventional PEFC. Fig. 9b shows that the output power of the conventional PEFC is significantly less sensitive to the GDL porosity than air-breathing PEFC; the conventional fuel cell very slightly improves with decreasing GDL porosity. This is primarily due to the high heat transfer coefficients that lead to relatively low temperatures for the conventional PEFC at low (~21 °C) and high (~26 °C) currents; see Fig. 9a. This situation, compared to that of the air-breathing PEFC, ensures lower saturation pressures of water vapour, higher water activity values (Fig. 9c), less ohmic losses (Fig. 9d) and ultimately that the fuel cell becomes less sensitive to GDL porosity and amount of water required for the humidification of the membrane phase.

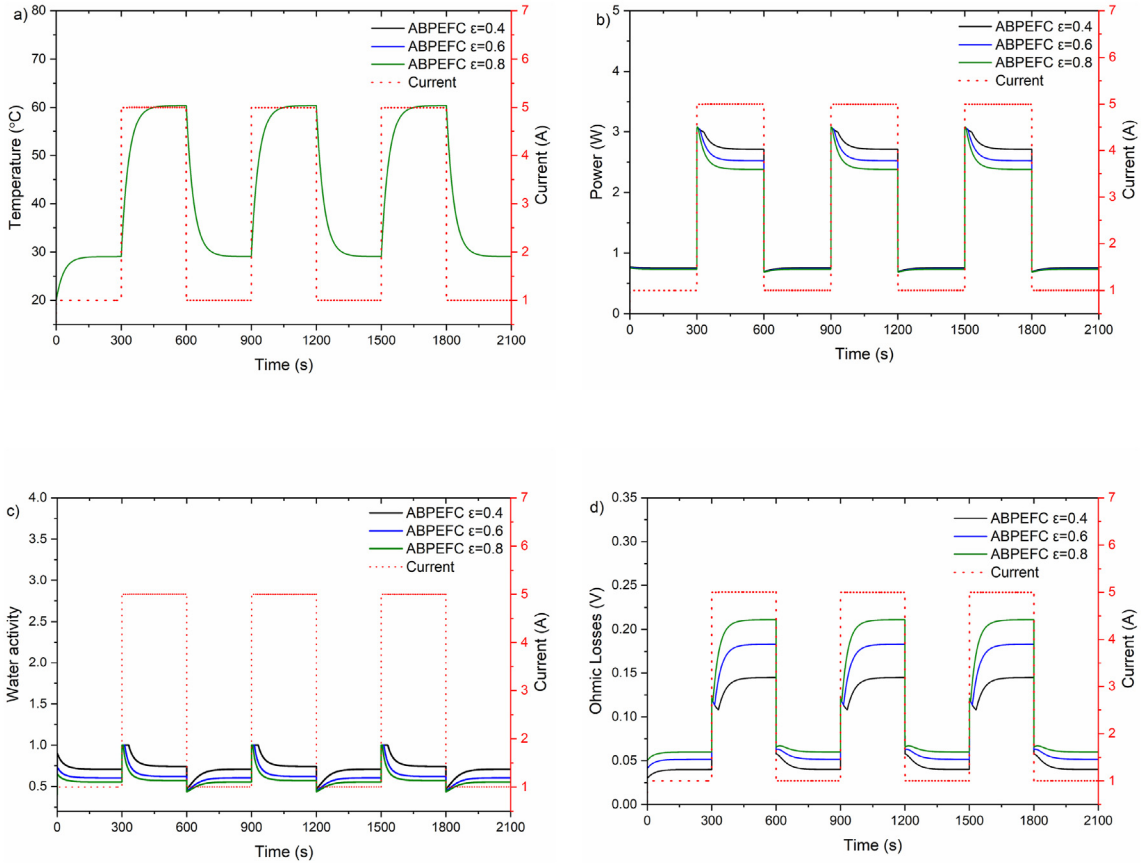

Fig. 8. Transient profiles of the modelled air-breathing PEFC for: (a) cell temperature, (b) output power, (c) water activity and (d) ohmic losses under different values for the GDL porosity at 20 °C and 40% relative humidity.

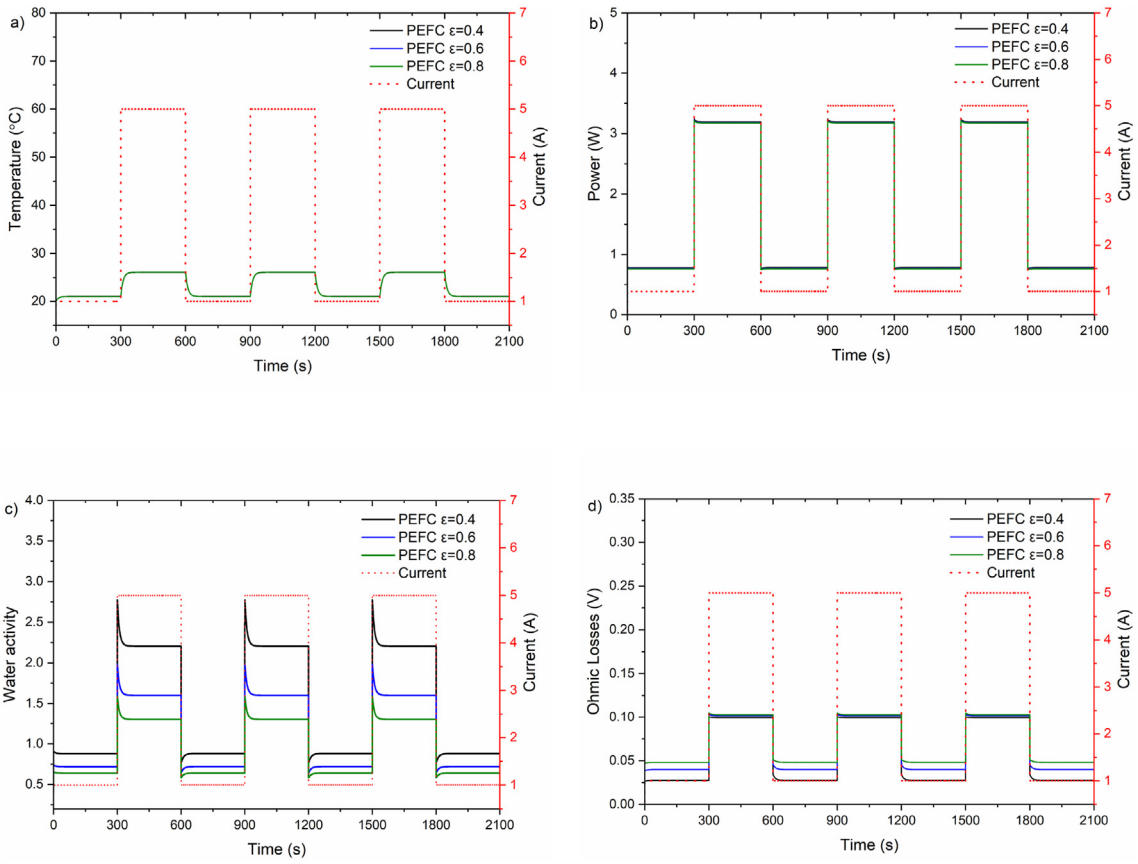

Fig. 9. Transient profiles of the modelled conventional PEFC for: (a) cell temperature, (b) output power, (c) water activity and (d) ohmic losses under different values for the GDL porosity at 20 °C and 40% relative humidity.

It is worth mentioning that the cell temperature profiles in Figs. 8 and 9 more or less overlap each other as the sensitivity of the cell temperature to the GDL porosity is almost negligible at 1 and 5 A. However, as shown in Fig. 3b in our previous work [18], the GDL porosity impacts the limiting current density which in turns impacts on the temperature of the fuel cells; this is particularly more evident for the air-breathing fuel cell. Namely, the lower is the porosity, the higher is the limiting current density and subsequently the higher is the cell temperature.

3.4. Membrane thickness effect

Fig. 10 and Fig. 11 show the impact of the membrane thickness on the dynamic and the steady-state performance of the air-breathing and conventional PEFCs, respectively. Overall, the figure expectedly demonstrates that the performance of the both types of the fuel cell improves with decreasing membrane thickness; however, the dynamic and the steady-state performances of the air-breathing PEFC is significantly more sensitive to the membrane thickness that the conventional PEFC; Figs. 10b and 11b. This is primary due to the poorer heat dissipation demonstrated by the air-breathing PEFC compared to the conventional PEFC; this is manifested through the significantly higher temperatures of the air-breathing PEFC; compare Figs. 10a and 11a.

As the membrane thickness increases, the ionic resistance of the membrane electrolyte increases (Eq. (15)) and subsequently the ohmic losses increases (Figs. 10d and 11d). This leads to an increased Joule heating (which is heat source and a product of the current density and the ohmic losses) and increased cell temperature (Figs. 10a and 11a). As the cell temperature increases, the activation losses in turn, as can be inferred from Eq. (13), increases; this could be clearly seen in Fig. 10c and to a much lesser extent in Fig. 11c.

3.5. Electrical resistance effect

Fig. 12 and Fig. 13 respectively show the impact of the lumped electrical resistance of all the electrically conducting components (i.e. the GDLs, the catalyst layers and the flow-field plates) on the dynamic and the steady-state performances of the modelled air-breathing and conventional PEFCs. As expected, the performance of both types of the fuel cell improves with decreasing the electrical resistance (Figs. 12b and 13b).

As with the impact of the membrane thickness, the increased electrical resistance leads to an increase in (i) the ohmic losses (Figs. 12d and 13d), (ii) the source term associated with the Joule heating, (iii) the cell temperature (Figs. 12a and 13a) and (iv) activation losses (Figs. 12c and 13c). For the given realistically selected ranges for the membrane thickness and the electrical resistance, the impact of the electrical resistance on either the dynamic or the steady-state performance of the fuel cell is less than that of the membrane thickness. Clearly, this is due to less ohmic losses obtained for the given values of the electrical resistance; compare for example Figs. 10d and 12d. For the same reason the impact of the electrical resistance appears to be quantitatively similar on the steady-state performance of the air-breathing and the conventional PEFCs.

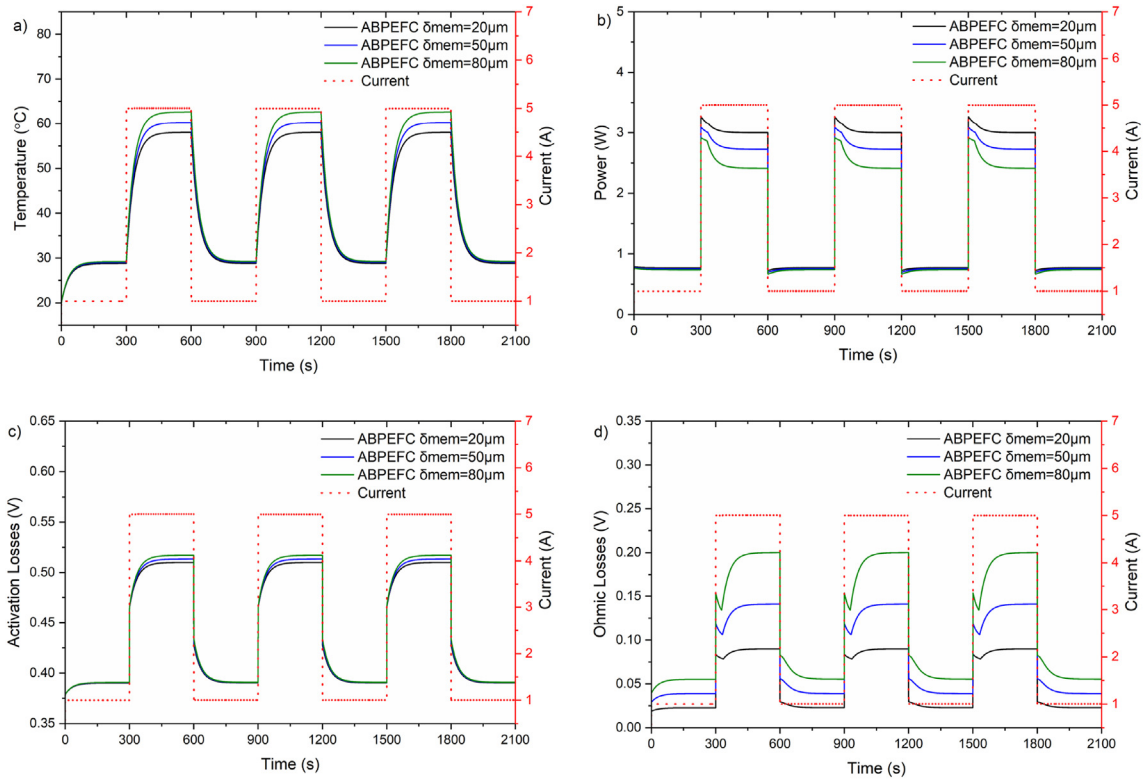

Fig. 10. Transient profiles of the modelled air-breathing PEFC for: (a) cell temperature, (b) output power, (c) activation losses and (d) ohmic losses under different values for the membrane thickness at 20 °C and 40% relative humidity.

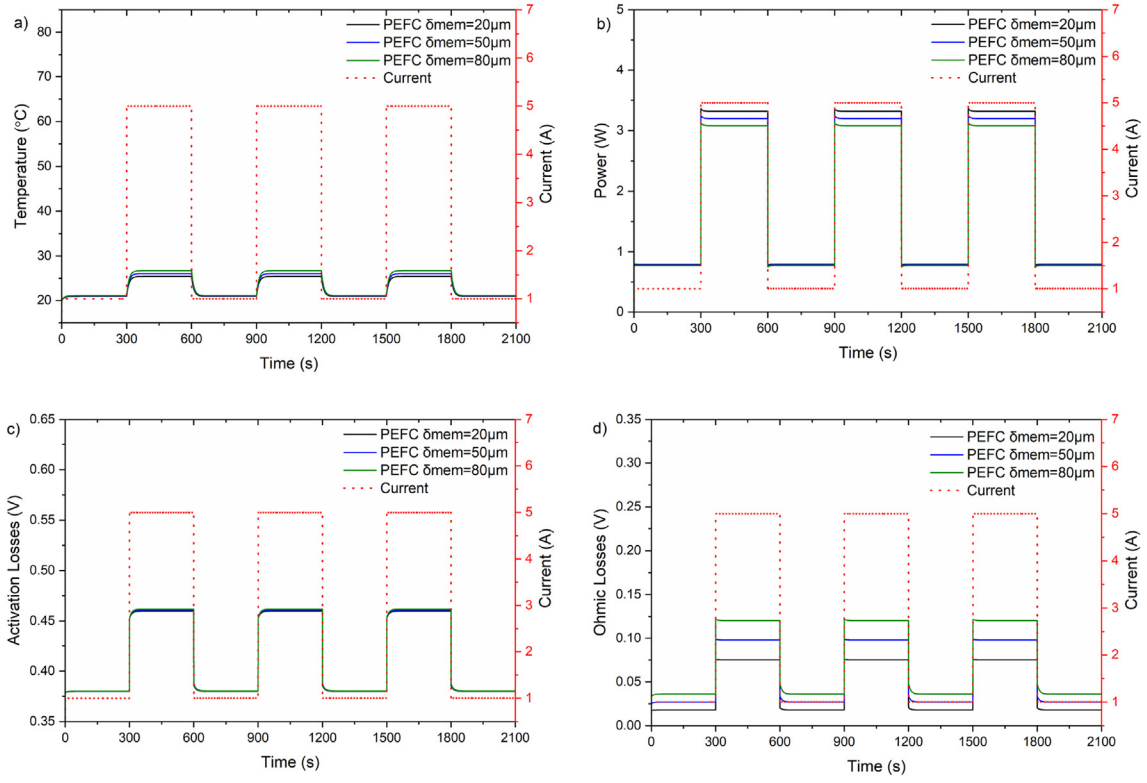

Fig. 11. Transient profiles of the modelled conventional PEFC for: (a) cell temperature, (b) output power, (c) activation losses and (d) ohmic losses under different values for the membrane thickness at 20 °C and 40% relative humidity.

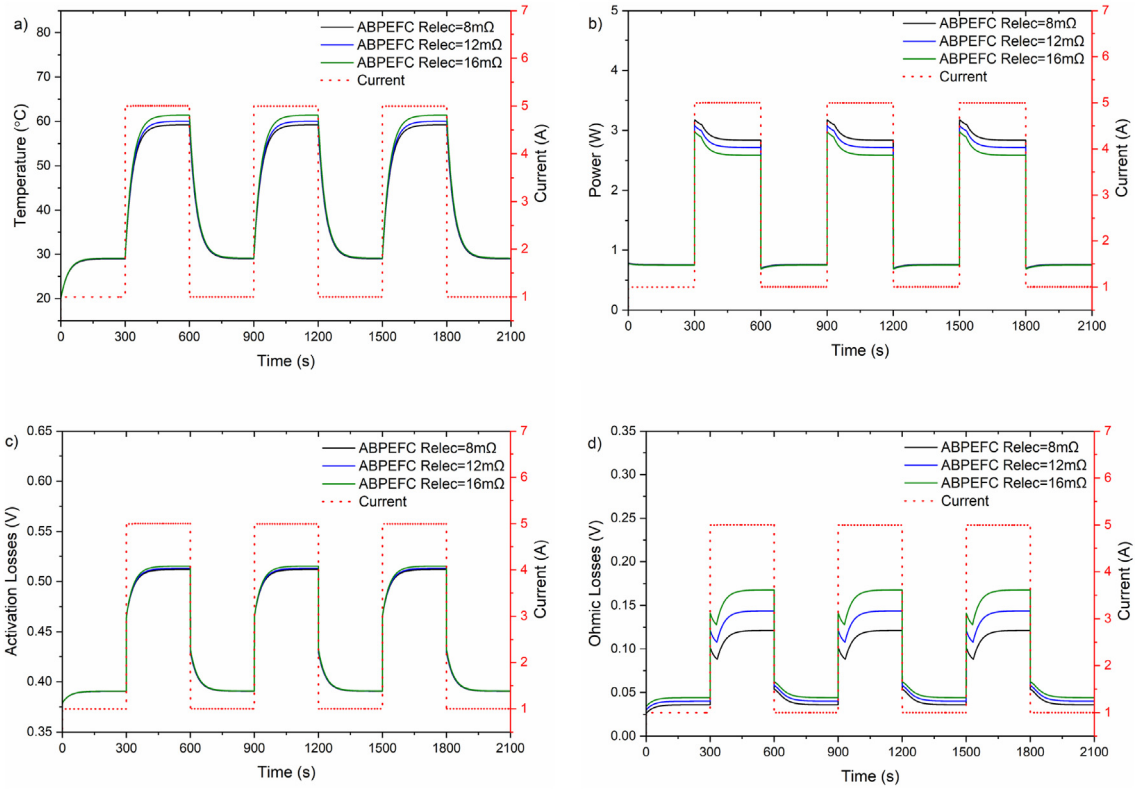

Fig. 12. Transient profiles of the modelled air-breathing PEFC for: (a) cell temperature, (b) output power, (c) activation losses and (d) ohmic losses under different values for the electric resistance at 20 °C and 40% relative humidity.

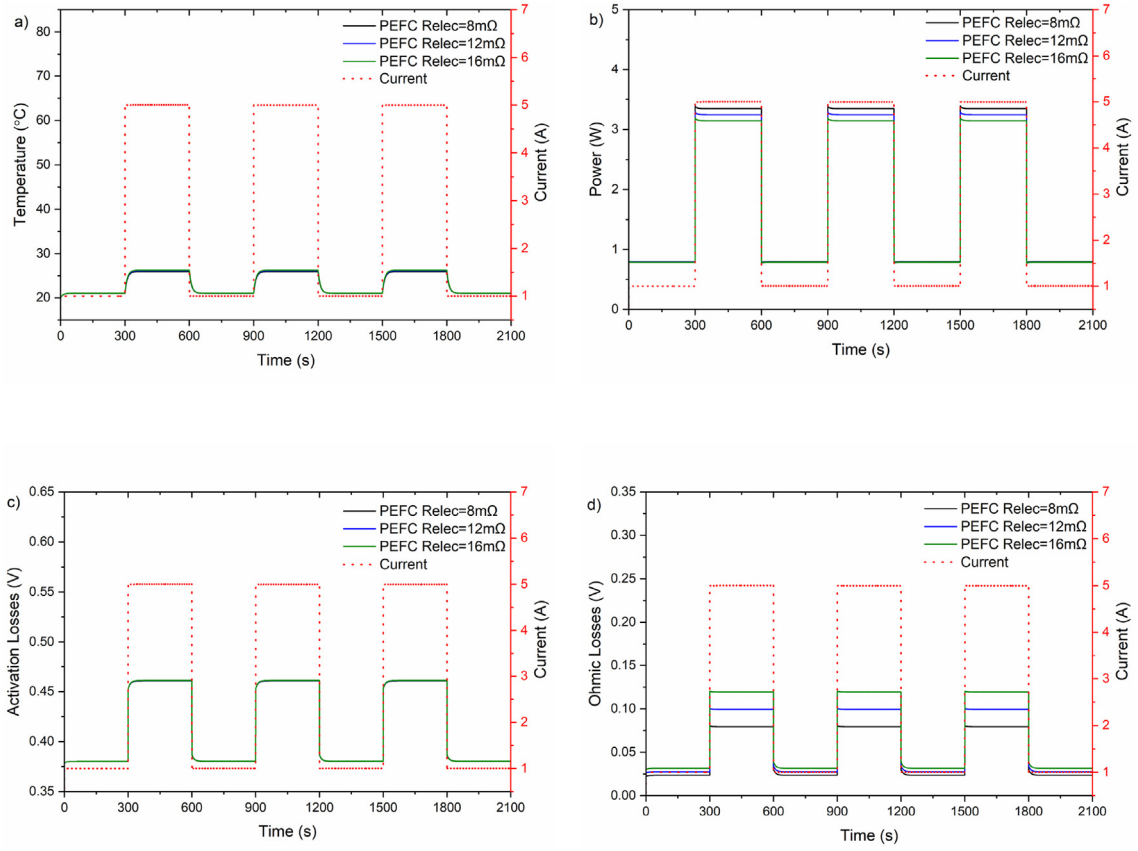

Fig. 13. Transient profiles of the modelled conventional PEFC for: (a) cell temperature, (b) output power, (c) activation losses and (d) ohmic losses under different values for the electric resistance at 20 °C and 40% relative humidity.

4. Conclusions

Two dynamic models have been developed for air-breathing and conventional PEFCs in order to investigate the sensitivity of the transient response and the performance of each type of the fuel cell to some key design parameters. This has been performed to obtain much better insights on how to improve the transient response of the air-breathing PEFC through comparing and contrasting the outcomes of its dynamic model with those of the dynamic model of the higher-in-performance and more responsive conventional PEFC. The following are the key findings of the study:

- The air-breathing PEFC is much less responsive to load changes than the conventional PEFC and this is primarily due to poor heat dissipation from the open cathode of the former type of the fuel cell caused by substantially lower natural convection-related heat transfer coefficients. This leads to significantly higher and less-responsive-to-load-changes cell temperature compared to the conventional PEFC and subsequently higher ohmic and activation losses.
- It is recommended that the porosity of the GDLs are designed to be relatively low to enhance the dynamic and the steady-state performances of the air-breathing PEFC. Higher GDL porosity values increases the removal rate of water required for the humidification of the membrane electrolyte, thus causing higher ohmic losses, significant overshoots with load alterations and poorer performance compared to lower GDL porosity values.
- The dynamic and the steady-state performance of the air-breathing PEFC improves with decreasing membrane thickness and, to a lesser extent, decreasing the overall electrical resistance. This is because the increase in the membrane thickness or electrical resistance leads to higher ohmic and activation losses. This impact is less profound on the performance of the conventional PEFC and this is clearly due to better heat dissipation demonstrated by this type of fuel cell.

CRediT authorship contribution statement

Fatma Calili-Cankir: Methodology, Software, Formal analysis, Investigation, Validation, Writing – original draft, Writing – review & editing, Visualization. **Mohammed S. Ismail:** Conceptualization, Methodology, Software, Formal analysis, Investigation, Validation, Writing – original draft, Writing – review & editing, Supervision. **Mohamed R. Berber:** Writing – review & editing, Funding acquisition. **Ziyad A. Alrowaili:** Writing – review & editing, Funding acquisition. **Derek B. Ingham:** Supervision, Writing – review & editing. **Kevin J. Hughes:** Supervision, Writing – review & editing. **Lin Ma:** Supervision, Writing – review & editing. **Mohamed Pourkashanian:** Supervision, Writing – review & editing, Project administration.

Declaration of competing interest

The authors declare that they have no known competing financial interests or personal relationships that could have appeared to influence the work reported in this paper.

Acknowledgements

The authors highly appreciate the Deputyship for Research & Innovation, Ministry of Education in Saudi Arabia for funding this work through the project number “375213500”. The authors extend their sincere appreciation to the central laboratory at Jouf University for supporting this study. Fatma Calili-Cankir thanks the Ministry of National Education at the Republic of Turkey for funding her PhD studentship at the University of Sheffield.

References

[1] W.R.W. Daud, R.E. Rosli, E.H. Majlan, S.A.A. Hamid, R. Mohamed, T. Husaini, PEM fuel cell system control: a review, Renewable Energy 113 (2017) 620–638, https://doi.org/10.1016/j.renene.2017.06.027.
[2] M. Dhimish, R.G. Vieira, G. Badran, Investigating the stability and degradation of hydrogen PEM fuel cell, International Journal of Hydrogen Energy 46 (74) (2021) 37017–37028, https://doi.org/10.1016/j.ijhydene.2021.08.183.
[3] Y. Qin, Q. Guo, R. Chen, Y. Zhuang, Y. Wang, Numerical investigation of water droplet impact on PEM fuel cell flow channel surface, Renewable Energy 168 (2021) 750–763, https://doi.org/10.1016/j.renene.2020.12.075.
[4] A. Solati, B. Nasiri, A. Mohammadi-Ahmar, K. Mohammadi, A.H. Safari, Numerical investigation of the effect of different layers configurations on the performance of radial PEM fuel cells, Renewable energy 143 (2019) 1877–1889, https://doi.org/10.1016/j.renene.2019.06.003.
[5] M. Rahimi-Esbo, A.A. Ranjbar, S.M. Rahgoshay, Analysis of water management in PEM fuel cell stack at dead-end mode using direct visualization, Renewable Energy 162 (2020) 212–221, https://doi.org/10.1016/j.renene.2020.06.078.
[6] A.M. Chaparro, P. Ferreira-Aparicio, Why portable electricity with hydrogen fuel cells?, in: Portable Hydrogen Energy Systems Academic Press, 2018, pp. 1–13, https://doi.org/10.1016/B978-0-12-813128-2.00001-2.
[7] T. Wilberforce, A. Alaswad, A. Palumbo, M. Dassisti, A.G. Olabi, Advances in stationary and portable fuel cell applications, International journal of hydrogen energy 41 (37) (2016) 16509–16522, https://doi.org/10.1016/j.ijhydene.2016.02.057.
[8] M.A.S. Al-Baghdadi, Performance comparison between airflow-channel and ambient air-breathing PEM fuel cells using three-dimensional computational fluid dynamics models, Renewable Energy 34 (7) (2009) 1812–1824, https://doi.org/10.1016/j.renene.2008.12.002.
[9] P.M. Kumar, A.K. Kolar, Effect of cathode channel dimensions on the performance of an air-breathing PEM fuel cell, International journal of thermal sciences 49 (5) (2010) 844–857, https://doi.org/10.1016/j.ijthermalsci.2009.12.002.
[10] W. Ying, J. Ke, W.Y. Lee, T.H. Yang, C.S. Kim, Effects of cathode channel configurations on the performance of an air-breathing PEMFC, International Journal of Hydrogen Energy 30 (12) (2005) 1351–1361, https://doi.org/10.1016/j.ijhydene.2005.04.009.
[11] S.U. Jeong, E.A. Cho, H.J. Kim, T.H. Lim, I.H. Oh, S.H. Kim, Effects of cathode open area and relative humidity on the performance of air-breathing polymer electrolyte membrane fuel cells, Journal of power sources 158 (1) (2006) 348–353, https://doi.org/10.1016/j.jpowsour.2005.09.044.
[12] P.W. Li, T. Zhang, Q.M. Wang, L. Schaefer, M.K. Chyu, The performance of PEM fuel cells fed with oxygen through the free-convection mode, Journal of Power Sources 114 (1) (2003) 63–69, https://doi.org/10.1016/S0378-7753(02)00535-9.
[13] D.T. Santa Rosa, D.G. Pinto, V.S. Silva, R.A. Silva, C.M. Rangel, High performance PEMFC stack with open-cathode at ambient pressure and temperature conditions, International Journal of Hydrogen Energy 32 (17) (2007) 4350–4357, https://doi.org/10.1016/j.ijhydene.2007.05.042.
[14] J. Fernández-Moreno, G. Guelbenzu, A.J. Martín, M.A. Folgado, P. Ferreira-Aparicio, A.M. Chaparro, A portable system powered with hydrogen and one single air-breathing PEM fuel cell, Applied energy 109 (2013) 60–66, https://doi.org/10.1016/j.apenergy.2013.03.076.
[15] P. Ferreira-Aparicio, A.M. Chaparro, Influence of the cathode architecture in the frequency response of self-breathing proton exchange membrane fuel cells, Journal of Power Sources 272 (2014) 79–89, https://doi.org/10.1016/j.jpowsour.2014.08.046.
[16] A. Kundu, J.H. Jang, J.H. Gil, C.R. Jung, H.R. Lee, S.H. Kim, B. Ku, Y.S. Oh, Micro-fuel cells—current development and applications, Journal of Power Sources 170 (1) (2007) 67–78, https://doi.org/10.1016/j.jpowsour.2007.03.066.
[17] T. Ous, C. Arcoumanis, The formation of water droplets in an air-breathing PEMFC, International journal of hydrogen energy 34 (8) (2009) 3476–3487, https://doi.org/10.1016/j.ijhydene.2009.02.037.
[18] F. Calili-Cankir, M.S. Ismail, D.B. Ingham, K.J. Hughes, L. Ma, M. Pourkashanian, Air-breathing versus conventional polymer electrolyte fuel cells: a parametric numerical study, Energy 250 (2022), 123827, https://doi.org/10.1016/j.energy.2022.123827.
[19] F. Calili, M.S. Ismail, D.B. Ingham, K.J. Hughes, L. Ma, M. Pourkashanian, A dynamic model of air-breathing polymer electrolyte fuel cell (PEFC): a parametric study, International Journal of Hydrogen Energy 46 (33) (2021) 17343–17357, https://doi.org/10.1016/j.ijhydene.2021.02.133.
[20] T. Fabian, J.D. Posner, R. O'Hayre, S.W. Cha, J.K. Eaton, F.B. Prinz, J.G. Santiago, The role of ambient conditions on the performance of a planar, air-breathing hydrogen PEM fuel cell, Journal of power Sources 161 (1) (2006) 168–182, https://doi.org/10.1016/j.jpowsour.2006.03.054.
[21] R. O'Hayre, T. Fabian, S. Litster, F.B. Prinz, J.G. Santiago, Engineering model of a passive planar air breathing fuel cell cathode, Journal of Power Sources 167 (1) (2007) 118–129, https://doi.org/10.1016/j.jpowsour.2007.01.073.
[22] M.S. Ismail, D.B. Ingham, K.J. Hughes, L. Ma, M. Pourkashanian, An efficient mathematical model for air-breathing PEM fuel cells, Applied energy 135

(2014) 490–503, https://doi.org/10.1016/j.apenergy.2014.08.113.
[23] F. Barbir, PEM Fuel Cells: Theory and Practice, Academic press, 2013.
[24] R. O'Hayre, S.W. Cha, W. Colella, F.B. Prinz, Fuel Cell Fundamentals, John Wiley & Sons, 2016.
[25] T. Yalcinoz, M.S. Alam, Dynamic modeling and simulation of air-breathing proton exchange membrane fuel cell, Journal of power sources 182 (1) (2008) 168–174, https://doi.org/10.1016/j.jpowsour.2008.03.076.
[26] J. Padulles, G.W. Ault, J.R. McDonald, An integrated SOFC plant dynamic model for power systems simulation, Journal of Power sources 86 (1–2) (2000) 495–500, https://doi.org/10.1016/S0378-7753(99)00430-9.
[27] Y. Sone, P. Ekdunge, D. Simonsson, Proton conductivity of Nafion 117 as measured by a four-electrode AC impedance method, Journal of the Electrochemical Society 143 (4) (1996) 1254, https://doi.org/10.1149/1.1836625.
[28] T.E. Springer, T.A. Zawodzinski, S. Gottesfeld, Polymer electrolyte fuel cell model, Journal of the electrochemical society 138 (8) (1991) 2334, https://doi.org/10.1149/1.2085971.
[29] M.Y. El-Sharkh, A. Rahman, M.S. Alam, P.C. Byrne, A.A. Sakla, T. Thomas, A dynamic model for a stand-alone PEM fuel cell power plant for residential applications, Journal of Power Sources 138 (1–2) (2004) 199–204, https://doi.org/10.1016/j.jpowsour.2004.06.037.
[30] H.I. Kim, C.Y. Cho, J.H. Nam, D. Shin, T.Y. Chung, A simple dynamic model for polymer electrolyte membrane fuel cell (PEMFC) power modules: parameter estimation and model prediction, International journal of hydrogen energy 35 (8) (2010) 3656–3663, https://doi.org/10.1016/j.ijhydene.2010.02.002.